THERMAL AND MECHANICAL ANALYSIS OF WELDED STRUCTURES*

R.E. NICKELL
Division of Engineering, Brown University, Providence, Rhode Island 02912, U.S.A.

H.D. HIBBITT
MarcAnalysis Research Corporation, Providence, Rhode Island 02906, U.S.A.

SUMMARY

The prediction of the residual state of stress and deformation in a welded structure is one of the most interesting, challenging and complex problems in structural mechanics. The wide spectrum of physical phenomena provides the interest; economic and safety considerations provide the challenge; and the essential nonlinearity of the analytical models provides the complexity.

Even if the prediction of the transient temperature field in the structure is assumed to be under control, determining the residual mechanical state is both a difficult and an expensive task. The analysis inevitably involves temperature-dependent mechanical properties and, in addition, the severe thermal gradients and high temperatures generic to the welding process induce irrecoverable inelastic creep and plasticity in the structure.

In spite of this, the stress analysis is now considered to be a straight forward application for general-purpose, nonlinear finite element structural programs. A few special features of such analyses, however, will be discussed: (1) the legitimacy of time-independent plasticity theories for treating the residual stress problem; (2) criteria for choosing plane stress, plane strain, generalized plane strain, or fully three-dimensional models; (3) methods for coping with possible floating regions (non-positive-definite stiffnesses) during cooling; and (4) the use of linear constraints to treat weld metal deposition and intermittent contact.

Since the most important parameters in the welding process that pertain to the stress analysis are the cooling rate and the welding torch efficiency, the heat transfer problem seems to require a critical look. The dominant features of this problem are: (1) source (torch) characterization; (2) radiation.from surfaces that are heated to high temperatures; (3) latent heat effects; and (4) subsidiary considerations, such as enforced convective heat transfer modes that are designed to control the cooling rate. Motion of the welding torch, even at low speeds, is not usually a critical factor in determining the residual mechanical state.

Again, finite element analysis is applicable, provided that the solution accuracy can be adequately estimated. Several alternative, two-step, implicit time integration schemes will be compared, especially with regard to accuracy and numerical stability for welding-type problems. The efficacy of "flux correction" will also be discussed. Then, the application of these ideas to typical industrial welding problems will be outlined.

* The support of Westinghouse, Bettis Atomic Power Laboratory, and the Office of Naval Research in the course of these investigations is gratefully acknowledged.

1. Introduction

The fabrication and integrity of large-scale structures, such as buildings, bridges, ships, pressure vessels, and other complex configurations, depends upon the use of reliable welding techniques. Although many of these techniques have been in use for decades, the quantitative aspects of the mechanics of welding have only recently received attention from analysts. Perhaps the most sophisticated work is that of Bjorhovde, et al. [1] who estimate the residual stresses in built-up sections (e.g., a building column) from the residual stress states in edge-welded and center-welded thick plates. An earlier analysis [2] used a rudimentary finite element program to compare against experimental results for thick sections.

Two fundamental shortcomings are inherent in this work: first, no attempt was made to quantify the thermal part of the problem (melting, solidification, and cooling rate); second, the restraint exerted by adjacent members during the welding process is extremely important in determining the residual stresses and deformations in a built-up structure. A more realistic approach for such welding problems is that of Hibbitt and Marcal [3], who analyze both the thermal and the mechanical parts of the welding problem with finite element methods. Rather than adopt the line-source solution to the heat transfer problem [4], a nonlinear transient finite element solution, including latent heat effects, material property temperature dependence, and thermal radiation boundary conditions, is obtained. This transient temperature distribution is then used as a forcing function for a finite element stress analysis, using incremental plasticity theory with temperature-dependent mechanical properties.

The findings in [3], although in conflict with published experimental results [5], confirmed the usual notions of residual stress states in welded parts [6]. First, the residual stress state for a "thin" welded section (here defined to be a fully fusion-penetrated section) exhibited plane stress characteristics, with the stress parallel to the welding path dominating. In the fusion zone this stress was tensile, with magnitudes approaching the room temperature yield strength. Substantial bending was observed in the section. Second, similar stress patterns were predicted for a "thick" welded section (partial fusion penetration), except that the plane stress behavior was no longer valid. High stresses corresponding to hydrostatic tension occurred at the root of the weld. These authors also modeled post-weld heat treatment by nonlinear creep and outlined a methodology for analytically treating weld dressing.

From the point of view of the designer trying to cope with void nucleation and fracture initiation in weldments, the standard guidelines are thus seen to be valid, but often impossible to implement. For instance, the welding sequence can be planned, in most cases, so that no additional tensile stress is imposed on the residual stress state; however, for indeterminate structures, the situation is so complex that an expensive analysis may be necessary. Preheating of thick sections, as recommended by the AWS Structural Welding Code, and post-weld heat treating are effective means of reducing the residual stresses (unless significant load is transferred to adjacent structure), but they are time-consuming and expensive. Stress concentration design features, such as notches, should be avoided near welds, insofar as possible, but many contemporary designs do not allow this luxury. Conservatism, utility and cost would seem to be pulling the designer

in different directions, therefore, and sophisticated analyses to determine the structural integrity of the weldment may be the only reasonable alternative.

As shown in [3], finding the residual mechanical state, although expensive, can be considered as a circumspect application for general-purpose, nonlinear finite element structural programs. An incremental, time-independent plasticity theory with temperature-dependent mechanical properties seems to be an adequate constitutive representation during the welding cycle, since the dominant stresses and distortions are induced at temperatures and over a time scale that inhibits significant creep. On the other hand, creep deformation and stress relaxation clearly dominate plasticity effects during post-weld heat treatment. Deformation arising during the molten state is commonly ignored.

Temperature increments from the welding thermal analysis must be selected with some caution in that large incremental changes in the mechanical state may result, with correspondingly inaccurate integration of the elastic-plastic rate equations. Computational accuracy is improved (and, therefore, somewhat larger temperature increments may be chosen) by incorporating "mean stiffness" and "mean normal" concepts [7], and by adding an out-of-equilibrium "residual load correction" [3] to successive increments.

The ultimate validity of the mechanical analysis will thus depend, in large measure, upon the validity of the solution to the thermal problem; the cooling rate and the welding arc efficiency will determine the extent of the fusion zone and the magnitude of the thermal gradients in the adjacent heat-affected zone, for example. Considering the critical nature of the thermal analysis, it is not clear that the computational techniques that are in general use today adequately treat this class of nonlinear, transient heat transfer problems.

2. Nonlinear Heat Transfer

The finite element method (FEM) has been used, for many years, to find approximate solutions to linear diffusion problems. Formulations have been based on several alternative global error distribution principles: (1) the concept of "restricted variation" [8], developed with FEM by Becker and Parr [9]; (2) conjugate field concepts [10] that have never achieved a great deal of popularity; (3) the transformed variational principle of Gurtin [11], developed with FEM by Wilson and Nickell [12]; and (4) the Galerkin method, a subclass of the method of weighted residuals (MWR), developed with FEM by Zienkiewicz and Parekh [13]. An excellent summary of the various approaches is contained in [14], where their equivalence for linear problems is pointed out.

As computational use of software based on these methods has increased, the need to extend program capability into the nonlinear regime has become evident. The nonlinearity manifests itself in three ways: (a) thermal property variation with temperature; (b) nonlinear boundary conditions, such as those associated with radiative heat transfer; and (c) phase transitions, such as melting and solidification. The latter is ordinarily treated as either a rapid change in effective specific heat between solidus and liquidus (a type (a) nonlinearity) or as an internal boundary condition that depends upon the temperature distribution (a type (b) nonlinearity).

From the very outset, finite element heat transfer programs that were based upon linear formulations were used to solve nonlinear problems, even though, strictly speaking, only the Galerkin method is easily extended to include nonlinear behavior. Usually the

thermal properties and the boundary conditions are estimated on the basis of the most recently computed temperatures (see [15] for an application to thermal radiation), a procedure that is best termed "quasi-linearization". The only apparent drawback to these ad hoc extensions into the realm of nonlinear analysis was an occasional numerical instability, even implicit, unconditionally stable time integration schemes (e.g., Crank-Nicolson) were being used. The common recourse was a smaller time step. Nevertheless, a sizable body of literature (e.g., [16,17]), citing good comparison with experimental results, has been accumulated through the use of quasi-linearization procedures.

More recently, some effort has been directed toward a rigorous understanding of the convergence and stability characteristics of the time integration schemes used in nonlinear, transient heat transfer analysis. An attempt to improve on the quasi-linearization procedure for nonlinear boundary conditions was reported in [18], where an "indirect iteration" algorithm was used. A classical paper by Douglas and Dupont [19], however, provides the proper framework for an all-inclusive approach to the question. In the following, their approach is recast in finite element form for clarity.

Assuming that a Galerkin approximation has been used to explicitly eliminate spatial dependence, in favor of a finite degree-of-freedom vector of time-dependent nodal point temperatures, $\underset{\sim}{\theta}(t)$, then a continuous time Galerkin representation of the nonlinear heat transfer problem is given by

$$\underset{\approx}{M}(\underset{\sim}{\theta}) \cdot \dot{\underset{\sim}{\theta}}(t) + \underset{\approx}{K}(\underset{\sim}{\theta}) \cdot \underset{\sim}{\theta}(t) = \underset{\sim}{Q}(\underset{\sim}{\theta},t) , \tag{1}$$

where $\underset{\approx}{M}(\underset{\sim}{\theta})$, $\underset{\approx}{K}(\underset{\sim}{\theta})$, and $\underset{\sim}{Q}$ are the temperature-dependent heat capacity matrix, conductivity matrix, and flux vector, respectively; t is the time; and a superposed dot represents a partial time derivative. If the problem happened to be linear, full or partial eigenvalue extraction ($\underset{\approx}{M}$ is positive definite; $\underset{\approx}{K}$ is positive semi-definite; therefore, all of the eigenvalues are real) would enable eq. (1) to be integrated precisely [20]. Such a procedure has been used by Guymon [21] for the linear, convective diffusion finite element formulation. There is also some evidence that this procedure is equally applicable to the nonlinear problem [22].

The Crank-Nicolson-Galerkin representation is found by solving eq. (1) at the middle of the time interval (t_n,t_{n+1}) and by evaluating the time derivative with a centered difference approximation

$$\dot{\underset{\sim}{\theta}}^a = \dot{\underset{\sim}{\theta}}(t^a) = (\underset{\sim}{\theta}_{n+1} - \underset{\sim}{\theta}_n)/\Delta t , \tag{2}$$

where $t^a = \frac{1}{2}(t_n+t_{n+1})$ and $\Delta t = t_{n+1} - t_n$. Therefore,

$$\left(\frac{2}{\Delta t}\underset{\approx}{M}(\underset{\sim}{\theta}^a) + \underset{\approx}{K}(\underset{\sim}{\theta}^a)\right) \cdot \underset{\sim}{\theta}_{n+1} = 2\underset{\sim}{Q}^a(\underset{\sim}{\theta}^a) + \left(\frac{2}{\Delta t}\underset{\approx}{M}(\underset{\sim}{\theta}^a) - \underset{\approx}{K}(\underset{\sim}{\theta}^a)\right) \cdot \underset{\sim}{\theta}_n , \tag{3}$$

where

$$\underset{\sim}{Q}^a(\underset{\sim}{\theta}^a) = \underset{\sim}{Q}(\underset{\sim}{\theta}^a,t^a) . \tag{4}$$

It should be noted that the separation of the flux vector into contributions at t_n and

t_{n+1} , i.e.,

$$\underset{\sim}{Q}^{a} = \frac{1}{2}\underset{\sim}{Q}_{n} + \frac{1}{2}\underset{\sim}{Q}_{n+1} , \tag{5}$$

is valid, in general, only for linear boundary conditions and source terms. Also, since neither $\underset{\sim}{\theta}^{a}$ nor $\underset{\sim}{\theta}_{n+1}$ are known, eq. (3) is a nonlinear, algebraic system of equations. Quasi-linearization would involve the evaluation of $\underset{\approx}{M}$, $\underset{\approx}{K}$ and $\underset{\sim}{Q}^{a}$, using the approximation $\underset{\sim}{\theta}^{a} = \underset{\sim}{\theta}_{n}$.

A generalized Crank-Nicolson-Galerkin representation can be found by using the same centered difference approximation for the time derivative but, instead, seeking the solution at some optimum point in the interval,

$$\underset{\sim}{\theta}^{o} = \frac{1}{2}(1+\gamma)\underset{\sim}{\theta}_{n+1} + \frac{1}{2}(1-\gamma)\underset{\sim}{\theta}_{n} , \tag{6}$$

where γ is the optimization parameter.

In this case

$$\left(\frac{2}{\Delta t}\underset{\approx}{M} + (1+\gamma)\underset{\approx}{K}\right)\cdot\underset{\sim}{\theta}_{n+1} = 2\underset{\sim}{Q}^{o} + \left(\frac{2}{\Delta t}\underset{\approx}{M} - (1-\gamma)\underset{\approx}{K}\right)\cdot\underset{\sim}{\theta}_{n} , \tag{7}$$

where $\underset{\approx}{M}$, $\underset{\approx}{K}$ and $\underset{\sim}{Q}^{o}$ are evaluated at $\underset{\sim}{\theta}^{o}$. If the heat capacity and conductivity do not depend upon temperature and the boundary conditions are nonlinear, then $\gamma = 1$ represents the indirect iteration scheme in [18]. There were also indications in [18] that $\gamma = 0.7$ represented an optimum point, at least for the class of problems being investigated. Note that the implicit coefficient matrix, $\left(\frac{2}{\Delta t}\underset{\approx}{M} + (1+\gamma)\underset{\approx}{K}\right)$, need be factored only once, unless the time step changes, while several iterations may be required at each time step for the solution vector to converge.

In order to avoid more than one iteration for the fully nonlinear problem, a predictor-corrector scheme can be employed with the generalized Crank-Nicolson-Galerkin representation. An intermediate temperature field, $\underset{\sim}{\theta}^{*}_{n+1}$, can first be found from eq. (7) with $\underset{\approx}{M}$, $\underset{\approx}{K}$, and $\underset{\sim}{Q}$ evaluated at $\underset{\sim}{\theta}_{n}$; then, $\underset{\sim}{\theta}_{n+1}$ is found, in the corrector step, from eq. (7) with the properties and boundary conditions evaluated at $\frac{1}{2}(1+\gamma)\underset{\sim}{\theta}^{*}_{n+1} + \frac{1}{2}(1-\gamma)\underset{\sim}{\theta}_{n}$ This scheme requires two factorizations per time step - an extremely expensive price to pay for accuracy.

Another scheme, which has been implemented in a general purpose finite element heat transfer program [3], is the Crank-Nicolson-Galerkin extrapolation. Here eq. (7) is solved with $\underset{\approx}{M}$, $\underset{\approx}{K}$ and $\underset{\sim}{Q}$ being evaluated at $\frac{3}{2}\underset{\sim}{\theta}_{n} - \frac{1}{2}\underset{\sim}{\theta}_{n-1}$ (a slight modification is required when the time step is changed). No corrector is used.

Douglas and Dupont [19] also recommend a predictor-corrector scheme that requires but one factorization per time step, making it nominally competitive with the extrapolation scheme. The corrector for one time step corresponds to the predictor for the next time step. For simplicity, the scheme will be described here with $\gamma = 1/2$. First, an intermediate field, $\underset{\sim}{\theta}^{*}_{n+1}$, is computed from eq. (7) with $\underset{\approx}{M}$, $\underset{\approx}{K}$ and $\underset{\sim}{Q}$ evaluated at $\frac{1}{2}(\underset{\sim}{\theta}^{*}_{n} + \underset{\sim}{\theta}_{n-1})$; then, the corrector field, $\underset{\sim}{\theta}_{n+1}$, is computed from eq. (7) with $\underset{\approx}{M}$, $\underset{\approx}{K}$ and $\underset{\sim}{Q}$ evaluated at $\frac{1}{2}(\underset{\sim}{\theta}^{*}_{n+1} + \underset{\sim}{\theta}_{n})$.

3. A Modified Operator

A modified Crank-Nicolson-Galerkin scheme can be derived by solving for the temperature at the middle of the time interval from eq. (3), but not extending the solution to the end of the interval. Then,

$$\left(\frac{2}{\Delta t}\,\underset{\sim}{M}(\underset{\sim}{\theta}^a) + \underset{\sim}{K}(\underset{\sim}{\theta}^a)\right) \cdot \underset{\sim}{\theta} = \underset{\sim}{Q}^a(\underset{\sim}{\theta}^a) + \frac{2}{\Delta t}\,\underset{\sim}{M}(\underset{\sim}{\theta}^a) \cdot \underset{\sim}{\theta}_n \,. \qquad (8)$$

The simplicity of eq. (8) is obvious and, it should be noted, all of the previously mentioned predictor-corrector and iterative rules still apply. This modified operator, similar to the original Crank-Nicolson scheme, can be shown to be unconditionally stable for linear problems.

For comparison, with regard to oscillation characteristics and stability limits, a one-dimensional, nonlinear example was solved with both eq. (3) and eq. (8), using extrapolation to estimate the fourth-power radiation boundary conditions. For the original Crank-Nicolson operator with lumped heat capacity, solutions were attempted for three different constant time step sizes: Δt = 50 sec., Δt = 200 sec., Δt = 1000 sec. The results are shown in Fig. 1. No significant oscillations are noted for Δt = 50 sec., indicating convergence to the correct solution; for Δt = 200 sec., some early oscillations are detected that gradually die out as steady state is reached; for Δt = 1000 sec., the solution diverges almost immediately. The same radiation problem was solved, with lumped heat capacity and identical time step sizes, using the modified operator. The results are shown in Fig. 2. An essentially identical solution was obtained for Δt = 50 sec.; for Δt = 200 sec., the solution does not oscillate and is bounded from above by the convergent solution; for Δt = 1000 sec., the solution displays slow divergence (see inset in Fig. 2) but remains bounded during the calculations. The modified operator would appear, on the basis of this limited study, to possess some distinct advantages over the conventional operator.

4. Welding Heat Transfer Example

In order to test the various time integration schemes on a typical welding heat transfer problem, the three potentially attractive candidates - quasi-linearization, extrapolation, and the Douglas-Dupont predictor-corrector - were used to solve a one-dimensional example involving temperature-dependent properties, nonlinear boundary conditions, and phase transition. A time-dependent surface heat flux was applied to a semi-infinite solid. The magnitude of the flux was determined from the parameters for a high-speed welding pass (14.5 volts, 300 amps, 15 in./min.) sufficient to create a partial fusion zone and bring about surface radiation, in addition to convective, cooling. The welding energy rate is, therefore, about 4 Btu/sec and 4 seconds are required to travel one inch (the high energy rate and welding speed are designed to accentuate differences in the time integration schemes).

The surface heat flux from the welding arc is assumed to be uniformly distributed in space (over a width equal to an electrode diameter) and normally distributed in time:

$$q(t) = q_o e^{-\frac{1}{2}\left(\frac{t-t_o}{\tau}\right)^2} \,, \qquad (9)$$

where q_o is the peak heat flux and τ is a characteristic time approximately equal to the time required for the bead to travel one electrode radius. The parameter t_o is chosen to be large enough that, essentially, all of the heat flux is accounted for by an analysis starting at time $t = o$. For this case, the electrode diameter was taken to be .05 in.; therefore, $\tau = 0.1$ sec. For t_o large enough, the total flux per unit length of weld is

$$\phi = 0.05\sqrt{\frac{\pi}{2}}\, q_o \tau . \tag{10}$$

For a weld efficiency of 50%, this would yield a peak heat flux of about 1000 Btu/in sec.

Ten first-order, plane isoparametric elements were used in the analyses. Each of the elements had dimensions equal to an electrode radius. The thermal properties for the material are given in Fig. 3. In addition to the variation in conductivity and specific heat with temperature, the density is 409 lb/ft^3 and two latent heat ranges were given - 18.2 Btu/lb at 1600°F and 108.7 Btu/lb at 3300°F. For this problem, the latent heat at 1600°F was treated as a local perturbation of the specific heat versus temperature curve. The cross-hatched area of Fig. 3 was calculated to be equal to 18.2 Btu/lb. The latent heat at 3300°F was treated in the conventional manner, with the solidus and liquidus assumed to be 3300°F and 3400°F, respectively. The emissivity used in the thermal radiation calculations and the convective heat transfer coefficient were selected as 0.9 and 5 Btu/ft^2hr, respectively.

For the first comparison q_o, τ and t_o were chosen to be 800 Btu/in^2sec, 0.1 sec and 0.3 sec., respectively. The surface temperature results, for a time step of 0.005 sec., are shown in Fig. 4. In all three analyses, the radiation cooling was treated implicitly; i.e., as a convective boundary layer with temperature-dependent boundary layer heat transfer coefficient,

$$h(T) = \varepsilon\sigma\left(T + T_\infty\right)\left(T^2 + T_\infty^2\right) , \tag{11}$$

where ε, σ and T_∞ are the emissivity, Stefan-Boltzmann constant, and sink temperature, respectively. The comparison of the three methods is favorable, although the surface temperature from quasi-linearization tends to wander as melting begins and also during the period when radiation plays an important role in surface heat transfer. Only slight differences are observed between the Douglas-Dupont predictor-corrector and extrapolation procedures.

The same problem was solved, using the predictor-corrector, with the radiation treated explicitly; i.e., as a prescribed surface heat flux. The drift of the solution away from the convergent result is shown in Fig. 5. The corrector does not improve the accuracy and, as noted in [18], several iterations would be required for convergence. If no other nonlinearities were present, indirect iteration would most likely be more efficient than an implicit treatment of the boundary condition; however, in the presence of material property temperature dependence and phase transitions, the implicit treatment is preferable.

A comparison between solutions for the same peak welding flux, but different characteristic times, is shown in Fig. 6. The extrapolation scheme was used for both analyses. Note that the peak flux is 100 Btu/in^2sec (a welding efficiency of less than 10%) in order to keep the surface temperatures down to reasonable levels. The effect of phase transition during both heating and cooling can be seen.

A final comparison is shown in Fig. 7. All three methods give virtually identical results except during rapid phase transition and in the period near peak surface temperatures. It is unlikely that any noticeable differences would occur during the remainder of the cooling part of the welding cycle.

On the basis of these results and comparisons, the time integration scheme that appears to blend accuracy and economy most favorably is the extrapolation method.

5. Omega Seal Weld Problem

The numerical approaches described previously have been applied to an omega seal during the first pass of a multi-pass welding operation in order to examine the residual distortion and stress associated with this flexible geometry. Such structural configurations are in common use for forming flexible, gas-tight seals between support structures and infrequently replaced components. The replacement sequence consists of flame-cutting to remove the old weld, joint preparation and rewelding of the newly-inserted component; therefore, prediction of weld distortion is required. The geometry in the case analyzed is axisymmetric; a radial cross section of the seal and its weld insert is shown in Fig. 8.

5.1 Thermal Analysis

Due to the mass of the parts adjacent to the omega seal, only the volume in and near the seal itself was modeled. Perfect kinematic restraint is assumed to be provided to the seal by these parts; in addition, the large heat sink is assumed to act as a semi-infinite medium. The weld insert geometry shown is valid prior to the first welding pass.

For this analysis, only the first pass of the sequence is being treated. The welding parameters for this pass are 9 volts, 74 amps, and a speed of 4.75 in/min. (the other three passes have twice the speed, the same voltage, and a current of 110 amps). The model of the welding process for this first pass is taken to be axisymmetric. Corrigan [5] has discussed the validity of this approach and has justified it experimentally. He reasons that, except for the start/stop point, each radial section of the configuration will experience the same thermal history and that the thermal diffusion ahead of the torch is not a controlling factor in comparison to the heat flux supplied by the torch itself. If the anomaly of the start/stop point is ignored, the speed of the first pass is sufficiently high, in comparison to the thermal diffusivity of metals, to justify the axisymmetric model.

The circumferentially uniform flux that is applied to the model is then assumed to be a normal distribution in space and time:

$$q(r,t) = q_o e^{-\frac{1}{2}\left(\frac{r-r_o}{\ell}\right)^2} e^{-\frac{1}{2}\left(\frac{t-t_o}{\tau}\right)^2}, \qquad (12)$$

where q_o is the peak heat flux for points on the weld centerline, r_o represents the radius of the weld centerline, and ℓ is a characteristic length approximately equal to an electrode radius. For this problem the total heat applied to the structure during the first pass is about 258 Btu, so that the peak flux can be found if the efficiency of the welding process can be estimated. The electrode diameter is 0.110 in. which implies that a characteristic length might be 1/16 in. and, with the arc speed of 4.75 in/min, a characteristic time would be about 3/4 sec. If the efficiency is assumed to be 75%, then

q_o is about 20 Btu/in.^{2} sec.

Thermal and mechanical material properties for the weld insert and the base metal (both were assumed to be constructed of Inconel 600) are shown in Figs. 9 and 10, respectively. The density is 0.304 lb/in.^{3}. Since no formal data on the latent heat values for Inconel 600 were available, the properties of nickel were used - the latent heat of fusion is about 133 Btu/lb for a material that is 72% Ni, 14-17% Cr, and 6-10% Fe; the solidus and liquidus were chosen to be 2470°F and 2575°F, respectively. In addition, the thermal conductivity was assumed to drop by 50% at melting while the specific heat rose by 15%.

Thermal radiation was also allowed for on all exposed surfaces, including those under the weld torch. The motivation here was to allow those heated surfaces to cool by radiating to cool surroundings (70°F) after the weld torch had passed. The remaining boundary condition concerned the conduction path to the massive heat sink. A simple one-dimensional conduction boundary layer model was used.

The thermal analysis of the omega seal was compared to two pieces of experimental evidence. Thermocouple data were available at the locations shown in Fig. 8. In addition, a photograph of a seal section (reproduced in Fig. 11) gave evidence of the extent of melting. Predicted isotherms at maximum extent of melting (3.5 seconds after onset of heating) are shown in Fig. 12 for purposes of comparison with the photograph; the comparison is favorable. Another favorable comparison, between the predicted thermal history and the thermal history and the thermocouple measurement at location 5 (Fig. 8) is shown in Fig. 13.

5.2 Stress Analysis

For the stress analysis, the same mesh was used as for the thermal analysis. Clamped boundary conditions were applied to the extremities of the omega seal. After cooling is complete, the residual hoop stress in and near the heat-affected zone is about 40-50 Ksi. The peak hoop stresses occur at a somewhat higher temperature and are shown in Fig. 14. At this temperature, the yield stress is about 40 Ksi. Predicted residual distortions compared poorly with experimental measurement because a flexible portion of the omega seal was omitted in the mechanical analysis.

Acknowledgment

The support of the Office of Naval Research in the course of these investigations is gratefully acknowledged.

References

[1] Bjørhovde, R.; Brozzetti, J.; Alpsten, G. A.; and Tall, L.; "Residual Stresses in Thick Welded Plates", Welding Journal 51, pp. 392-s - 405-s (1972).

[2] Brozzetti, J.; Alpsten, G. A.; and Tall, L.; "Welding Parameters, Thick Plates, and Column Strength", Welding Journal 50, pp. 331-2 - 342-s (1971).

[3] Hibbitt, H. D. and Marcal, P. V., "A Numerical Thermo-Mechanical Model for the Welding and Subsequent Loading of a Fabricated Structure", Computers and Structures (in press).

[4] Dorschu, K. E., "Control of Cooling Rates in Steel Weld Metal", Welding Journal 47, pp. 49-s - 62-s (1968).

[5] Corrigan, D. A., "Thermomechanical Effects in Fusion Welding of High Strength Steels", Ph.D. Dissertation, MIT (1966).

[6] Masubuchi, K., "Control of Distortion and Shrinkage in Welding", Welding Research Council Bulletin No. 149, New York, 1970.

[7] Rice, J. R. and Tracey, D. M., "Computational Fracture Mechanics", ONR Symposium on Numerical and Computer Methods in Structural Mechanics, Urbana, Illinois, 1971.

[8] Rosen, P., "On Variational Principles for Irreversible Processes", J. Chem. Phys. 21, pp. 1220-1221, 1953.

[9] Becker, E. B. and Parr, C. H., "Application of the Finite Element Method to Heat Conduction in Solids", Tech. Report S-117, Rohm & Haas Company, 1968.

[10] Morse, P. M. and Feshbach, H., Methods of Theoretical Physics. Volume I, McGraw-Hill, New York, 1953.

[11] Gurtin, M. E., "Variational Principles for Linear Initial-Value Problems", Quart. Appl. Math. 22, pp. 252-256, 1964.

[12] Wilson, E. L. and Nickell, R. E., "Application of the Finite Element Method to Heat Conduction Analysis", Nucl. Engr. Des. 4, pp. 276-286, 1966.

[13] Zienkiewicz, O. C. and Parekh, C. J., "Transient Field Problems - Two-Dimensional and Three-Dimensional Analysis by Isoparametric Finite Elements, Int. J. Numer. Meth. Engr. 2, pp. 61-71, 1970.

[14] Finlayson, B. A., The Method of Weighted Residuals and Variational Principles, Academic Press, New York, 1972.

[15] Richardson, P. D. and Shum, Y. M., "Use of Finite Element Method in Solution of Transient Heat Conduction Problem", ASME Paper 69-WA/HT-36.

[16] Jaeger, R. E. and Nickell, R. E., "Thermal Shock Resistant Zirconia Nozzles for Continuous Copper Casting", in: Materials Science Research 5, pp. 163-184, ed. by W. W. Kriegel, Plenum Publishing Co., New York (1971).

[17] Dunn, J. C. and Nickell, R. E., "Reentry Thermal Analysis of Variable Thickness Spherical Vehicles", in: Progress in Astronautics and Aeronautics 29 - Fundamentals of Spacecraft Thermal Design, pp. 319-331, ed. by J. W. Lucas, MIT Press, Cambridge (1972).

[18] Chu, S. C. and Yalamanchili, R. V. S., "Application of the Finite-Element Method to Heat-Transfer Problems. Part I. Finite-Element Method Applied to Heat-Conduction in Solids with Nonlinear Boundary Conditions", Technical Report RE TR 71-37, U.S. Army Weapons Command (1971).

[19] Douglas, Jr., J. and Dupont, T., "Galerkin Methods for Parabolic Equations", SIAM J. Numer. Anal. 7, pp. 575-626 (1970).

[20] Dunham, R. S., Nickell, R. E., and Stickler, D. C. "Integration Operators for Transient Structural Response", Computers and Structures 2, pp. 1-15 (1972).

[21] Guymon, G. L., "A Finite Element Solution of the One-Dimensional Diffusion-Convection Equation", Water Resources Res. 6, pp. 204-210 (1970).

[22] Destefano, G. P., "Causes of Instabilities in Numerical Integration Techniques", Int. J. Comp. Math. 2, pp. 123-142 (1968).

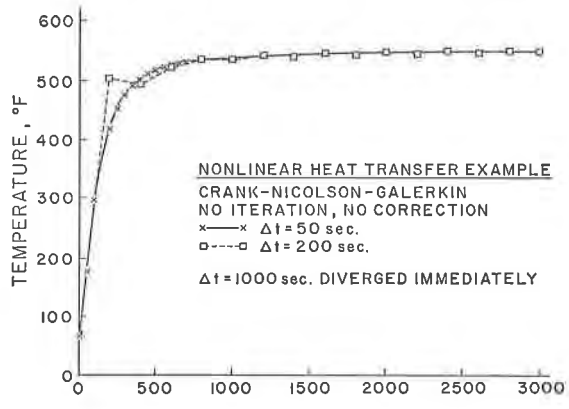

Fig. 1. Crank-Nicolson-Galerkin Nonlinear Radiation Example.

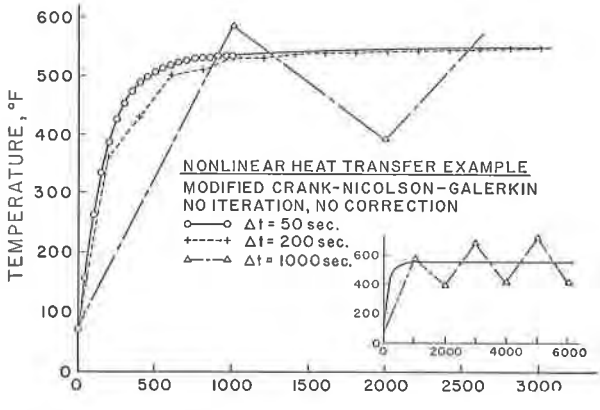

Fig. 2. Modified Crank-Nicolson-Galerkin Nonlinear Radiation Example.

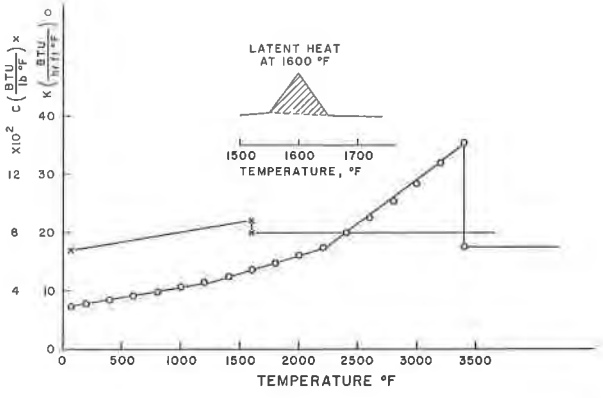

Fig. 3. Thermal Properties - One Dimensional Welding Example.

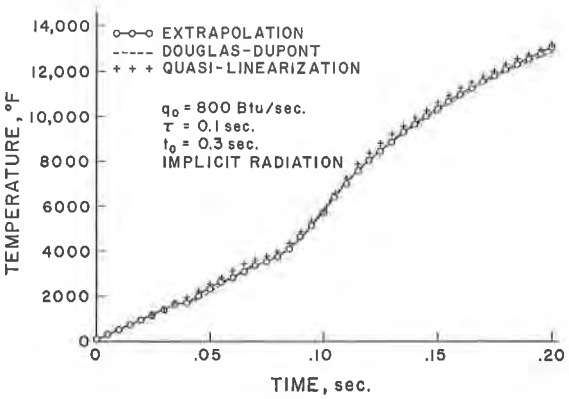

Fig. 4. Comparison of Three Temporal Operators, One-Dimensional Welding Example, High Heat Flux.

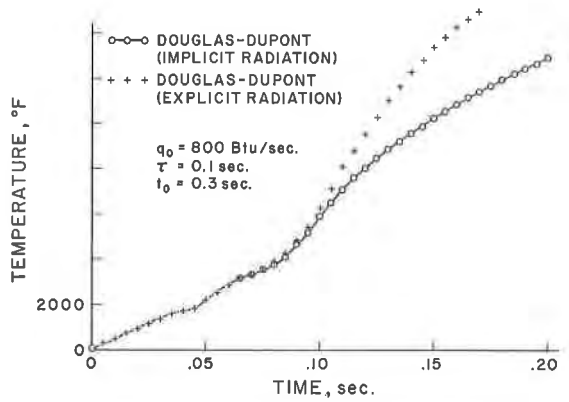

Fig. 5. Implicit vs. Explicit Radiation, Douglas-Dupont Predictor Corrector.

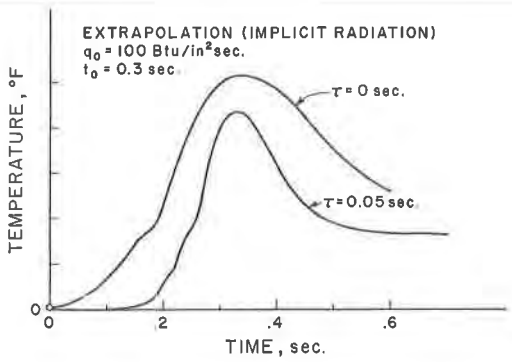

Fig. 6. Characteristic Time Comparison, Extrapolation Method.

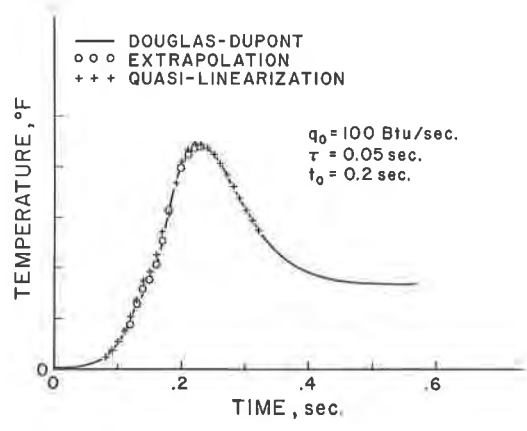

Fig. 7. Comparison of Three Temporal Operators, One-Dimensional Welding Example, Low Heat Flux.

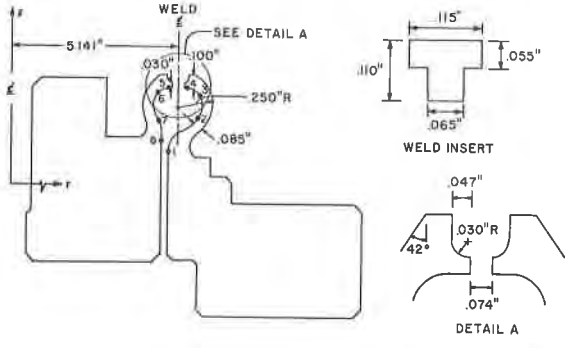

Fig. 8. Omega Seal Geometry and Thermocouple Placement.

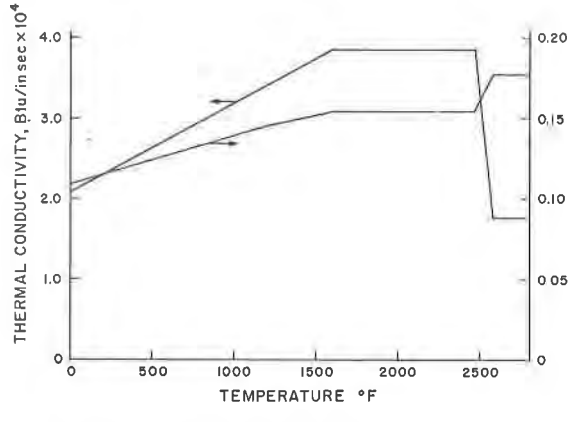

Fig. 9. Inconel Thermal Properties vs. Temperature.

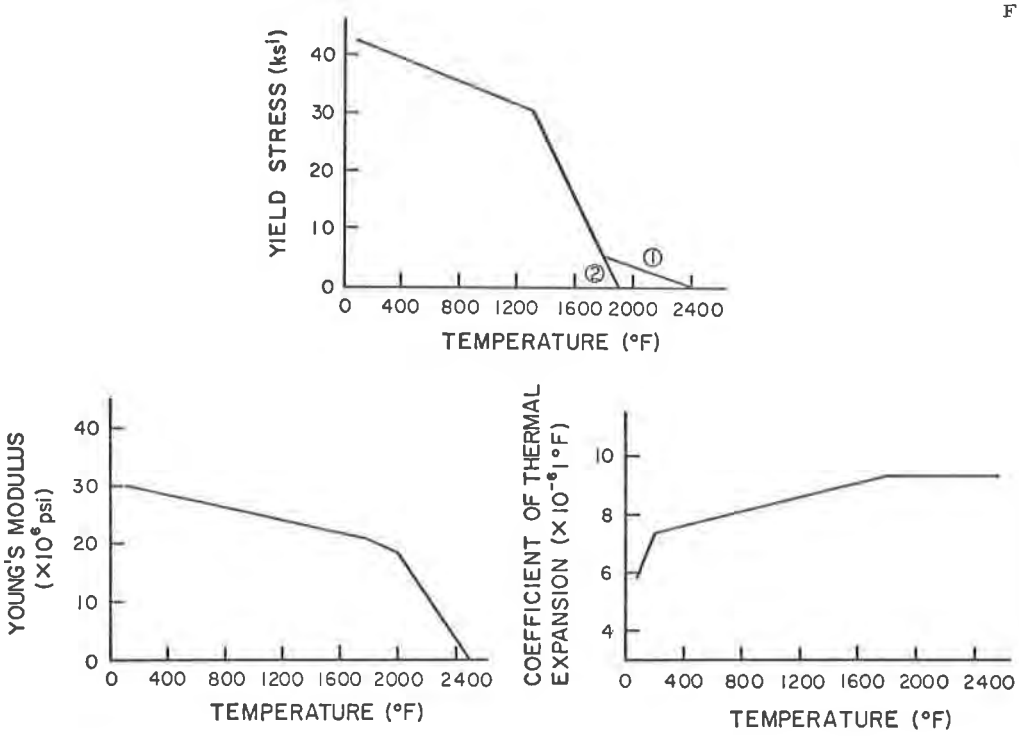

Fig. 10. Inconel Mechanical Properties vs. Temperature.

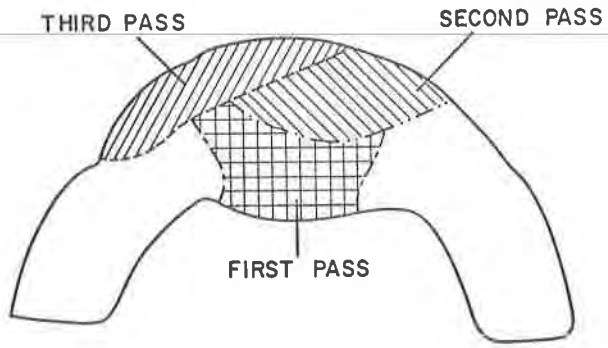

Fig. 11. Observed Melt Regions (From Photograph) Omega Seal.

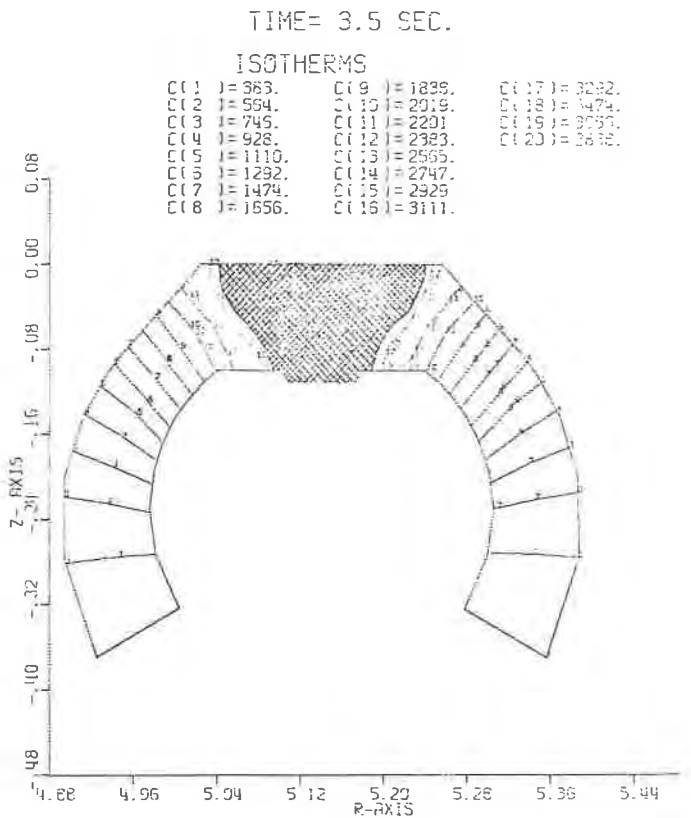

Fig. 12. Predicted Melt Region, First Pass, Omega Seal.

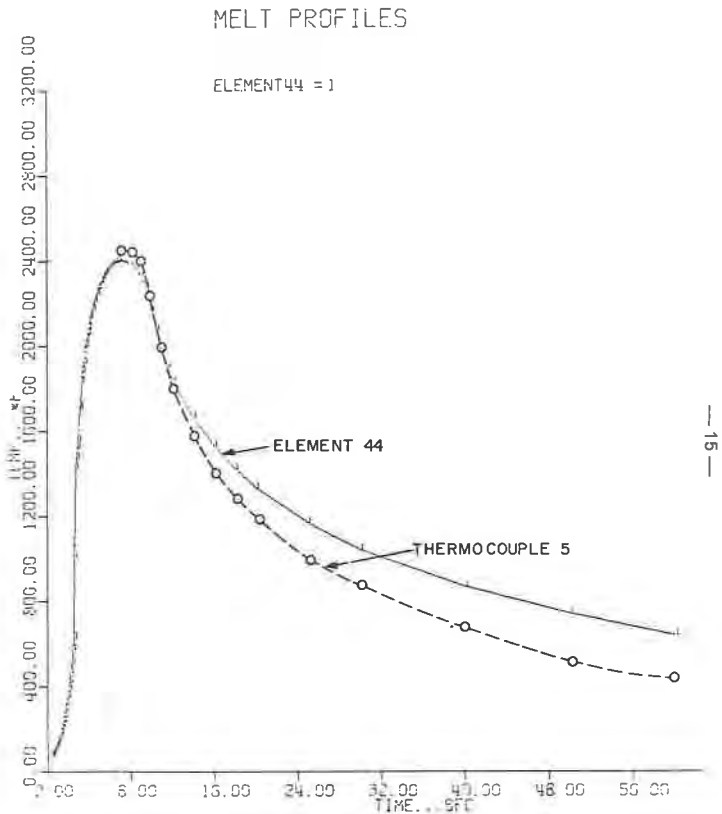

Fig. 13. Thermocouple Comparison, Heat-Affected Zone.

F 6/1

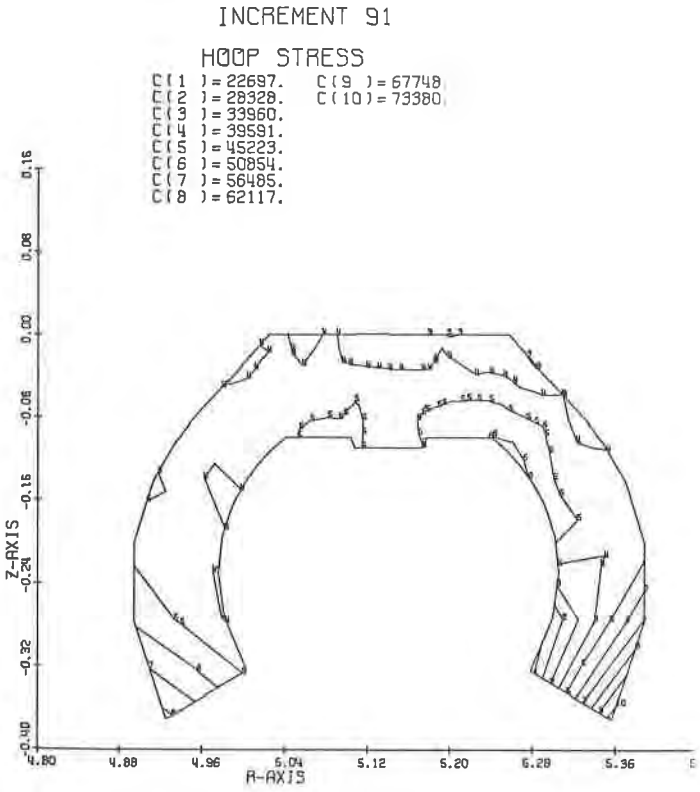

Fig. 14. Residual Circumferential Stress Contours.